Characterizations of geothermal springs along the Moxi deep fault in the western Sichuan plateau, China

CrossMark

Jihong Qi [a], Mo Xu [a,*], Chengjiao An [a], Mingliang Wu [a], Yunhui Zhang [a], Xiao Li [a], Qiang Zhang [a], Guoping Lu [b]

[a] State Key Laboratory of Geohazard Prevention and Geoenvironment Protection, Chengdu University of Technology, Chengdu 610059, China
[b] School of Environmental Studies, China University of Geosciences, Wuhan 430074, China

A B S T R A C T

Abundant geothermal springs occur along the Moxi fault located in western Sichuan Province (the eastern edge of the Qinghai-Tibet plateau), highlighted by geothermal water outflow with an unusually high temperature of 218 °C at 21.5 MPa from a 2010-m borehole in Laoyulin, Kangding. Earthquake activity occurs relatively more frequently in the region and is considered to be related to the strong hydrothermal activity. Geothermal waters hosted by a deep fault may provide evidence regarding the deep underground; their aqueous chemistry and isotopic information can indicate the mechanism of thermal springs. Cyclical variations of geothermal water outflows are thought to work under the effect of solid earth tides and can contribute to understanding conditions and processes in underground geo-environments. This paper studies the origin and variations of the geothermal spring group controlled by the Moxi fault and discusses conditions in the deep ground. Flow variation monitoring of a series of parameters was performed to study the geothermal responses to solid tides. Geothermal reservoir temperatures are evaluated with Na-K-Mg data. The abundant sulfite content, dissolved oxygen (DO) and oxidation-reduction potential (ORP) data are discussed to study the oxidation-reduction states. Strontium isotopes are used to trace the water source. The results demonstrate that geothermal water could flow quickly through the Moxi fault the depth of the geothermal reservoir influences the thermal reservoir temperature, where supercritical hot water is mixed with circulating groundwater and can reach 380 °C. To the southward along the fault, the circulation of geothermal waters becomes shallower, and the waters may have reacted with metamorphic rock to some extent. Our results provide a conceptual deep heat source model for geothermal flow and the reservoir characteristics of the Moxi fault and indicate that the faulting may well connect the deep heat source to shallower depths. The approach of hot spring variation research also has potential benefits for earthquake monitoring and prediction.

© 2017 Elsevier B.V. All rights reserved.

1. Introduction

Hydrothermal activities have a very close relationship with deeply cut and elongated fault zones (Arancibia et al., 2014; Humphris et al., 2015; Khaska et al., 2015; Khutorskoi and Polyak, 2014; Navarro-Ciurana et al., 2016; Rissmann et al., 2011), while geothermal waters move along fast flow paths associated with the faulting. Thermal springs can have various heat sources, such as volcanoes, magmatic intrusions and radioactivity (Guo and Wang, 2012; Mohammadi et al., 2010). The geothermal waters are mainly derived from meteoric water and their chemistry is influenced by tectonic activity, rocks and deep fluids (Capecchiacci et al., 2015; Kaasalainen et al., 2015; Kalacheva et al., 2015; Lee et al., 2011; Shakeri et al., 2015; Yaguchi et al., 2014).

Regional structural stress fields changed by earthquakes can also cause variation of the hydrochemical components. Therefore, research on hydrochemical components in fault zones has attracted many scholars (Khaska et al., 2015; Mao et al., 2015; Luo and Liu, 2010). Most publications have focused on the geochemistry and isotopic composition of both water and gas to trace the origin of the water (Tassi et al., 2010; Phuong et al., 2012; Yaguchi et al., 2014). In addition, earthquake prediction can be facilitated by geochemical indicators in hot springs, such as rations of anion/cation, D and ^{18}O isotopes, and gas components (Cao et al., 2006; Reed, 1982; Wang et al., 2013; Pang et al., 2013). Recently, the monitoring of variations in flow has been applied to explain the mechanical process and predict earthquakes (Luo and Liu, 2010; Shi and Wang, 2013).

In the western Sichuan plateau, the Xianshuihe strike-slip fault extending more than 200 km is a major regional fault of longitudinally aligned tectonics in China. It meets the Longmenshan Fault and the Anninghe Fault in the area from Kangding to Simian (Fig. 1a), where it could reach as deeply as to the Moho surface (Zhang, 1978). These three faults, expected to extend to the asthenosphere, are active at present (Shan et al., 2013; Li and Shibazaki, 2014; Shao et al., 2016). The intersection zone is located in the southwestern Sichuan plateau, where the northward-moving Indian block causes the Tibetan Plateau to collide beneath the Yangtze Block, which plays a dominant role in crustal movements in China.

Due to the long-term and frequent tectonic movements, the intersection marks a complicated crustal structure and intensive structural deformation. Recently, the Kangding M6.3 earthquake and the Lushan M7.0 earthquake occurred in 2014 and 2013 respectively, under the influence of the active neotectonics in this area (Liu et al., 2016; Zhang et al., 2016). This area also possesses abundant geothermal resources, which include one of the main geothermal zones in southern China belonging to the Mediterranean-Himalayas geothermal belt (Guo and Wang, 2012; Liao and Zhao, 1999). The fault is divided into four segments: the Qianning fault (F_{1-1}), the Yalahe fault (F_{1-2}), the Selaha fault (F_{1-3}) and the Moxi fault (F_{1-4}); according to the evolution of the fault (An, 2010), the Moxi segment passes through Kangding to Shimian (Fig. 1a).

However, little research has been carried out to date especially in terms of earthquake implications from geothermal spring activity. Only the hydrochemical and gas components of several thermal springs appearing north of Kangding have been discussed. With the methods of Ryzner's index and Larson's index, and the Na-K-Mg equilibrium diagram, certain thermal groundwater in several of the geothermal wells and hot springs in the Kangding area has shown a tendency to scale (Wei et al., 2012). The gas geochemical characteristics were investigated for the seismic belts in western Sichuan, including the data of the chemical components and the isotopic ratios of helium, neon and carbon in many samples; stable carbon isotopes of CO_2 gas showed that the spring gases have multiple sources (Zhou, 2011). The stable carbon isotopes of the hot water and limestone in Kangding indicated that the deep-source CO_2 is of the mantle origin or metamorphic origin or a mixture (Yang et al., 1999).

The geothermal system in western Sichuan is relatively less studied, compared with other tectonically active areas such as Yunnan and Guangdong Province. Using the enthalpy relative to chloride for hot springs in the Tengchong hydrothermal areas, southwestern China, it has been concluded that the parent geothermal liquid ascends to the surface through different channels (Guo, 2012; Guo and Wang, 2012). Studying the geochemical and isotopic characteristics hosted by deep-seated faults in Dongguan Basin, South China, suggests that the groundwater is migrating and being heated very quickly in a relatively fast conductive fracture system (Mao et al., 2013). The multi-parameter automatic gas monitoring results are considered to be sensitive to the local crustal stress and valuable for conducting real-time monitoring of seismo-geochemical precursors (Yang et al., 2006).

This paper discusses the geothermal system of the Moxi fault in terms of the aqueous chemistry of geothermal waters based on physical and chemical parameters. With the interpretation of water-rock reaction and geothermal reservoir, it attempts to trace the origin of the heat. Meanwhile, it studies the daily variations of flow in views of solid tides. All of the work above are expected to reveal relationship between regional fault zones and the geothermal system that could contribute to earthquake predictions.

2. Geological setting and concept model

2.1. Geological settings

Our study focuses on the geothermal springs associated with the Moxi fault, which is the southern part of the Xianshuihe Fault from Laoyulin to Shimian (Fig. 1a). The Moxi fault extends roughly in a SE direction for approximately 55 km and dips steeply toward the west. Two other small faults are prominent. One is the Detuo fault. which goes northeastward and cuts the south end of the Moxi fault at the mouth of river Shiyuehe. The other is the Hailuogou fault, which extends latitudinally and crosses the Moxi fault at Hailuogou (Fig. 1b).

The study area is mainly covered by Permian metamorphic rock, crystalline limestone and magmatic rocks of the Proterozoic (Jinning), Indosinian and Himalayan periods. Intrusive rocks are largely distributed along the Moxi fault. Bounded by this fault, the Proterozoic magmatic rocks are found in the footwall, while Indosinian and Himalayan granites are mainly located in the hanging wall. However, the Permian metamorphic rock and crystalline limestone are exposed mostly to the west of the Moxi fault, from around the Laoyulin area to Simian, neighboring the younger granite.

Accompanying the Detuo fault, more secondary faults developing from the Moxi fault appear, and exposure of strata becomes more complex in the intersection. As a result, Paleozoic Devonian strata appear, which are metamorphosed to a certain degree.

The Dadu River is the main river flowing south, which developed along the Detuo fault. Meanwhile, there are several minor rivers flowing west-eastward, which probably developed along several small faults; for example, the Hailuogou river flows along the Hailuogou fault.

2.2. Sample description

It is interesting that the borehole or natural springs are mostly distributed to the west of the Moxi fault, which is the hanging wall of this fault. Geothermal springs are naturally exposed along the Moxi fault, usually appearing on the bank of sub-rivers which are expected to be controlled by the sub-faults.

The Laoyulin geothermal field in Kangding shows intensive geothermal activity (Sheng, 2007; Cao et al., 2006; Zhao, 1984) from the level of Himalayan magmatic rocks. In this area, maximum spring temperatures can reach 81 °C, nearly the local boiling temperature, and the lowest temperature is only 28 °C.

Borehole drilling in Laoyulin revealed unusual intensity in the geothermal waters, with outflows at 218 °C and 21.5 MPa pressure. Borehole ZK3 was drilled down to a depth of 2010 m and unleashed geothermal water by breaking through the fault zone.

Approximately 12 km south of Yulingong, the Mount Jianjian warm spring at 47 °C occurs at the boundary of the Quaternary deposits and the Late Permian metamorphic rock, with a flow rate approximately 1.46 L/s, and a strong sulfur odor. Meanwhile the Quaternary deposits distributed through the valley developing along the Moxi fault.

On the banks of the Hailuogou river, which is approximately 10 km south of Mount Jianjian, many geothermal springs emerge, and two sampling sites were investigated. One is at 62 °C high, and the other is at approximately 59 °C near the river, both of them have a strong sulfur odor. In this zone, Mesozoic strata and Permian metamorphic rocks are both exposed. In fact, samples were taken along the boundary between these two types of rocks.

Another three samples were obtained near the intersection of the Moxi and Detuo faults, collected on the bank of a sub-river where Paleozoic Devonian strata are exposed. Wandong spring
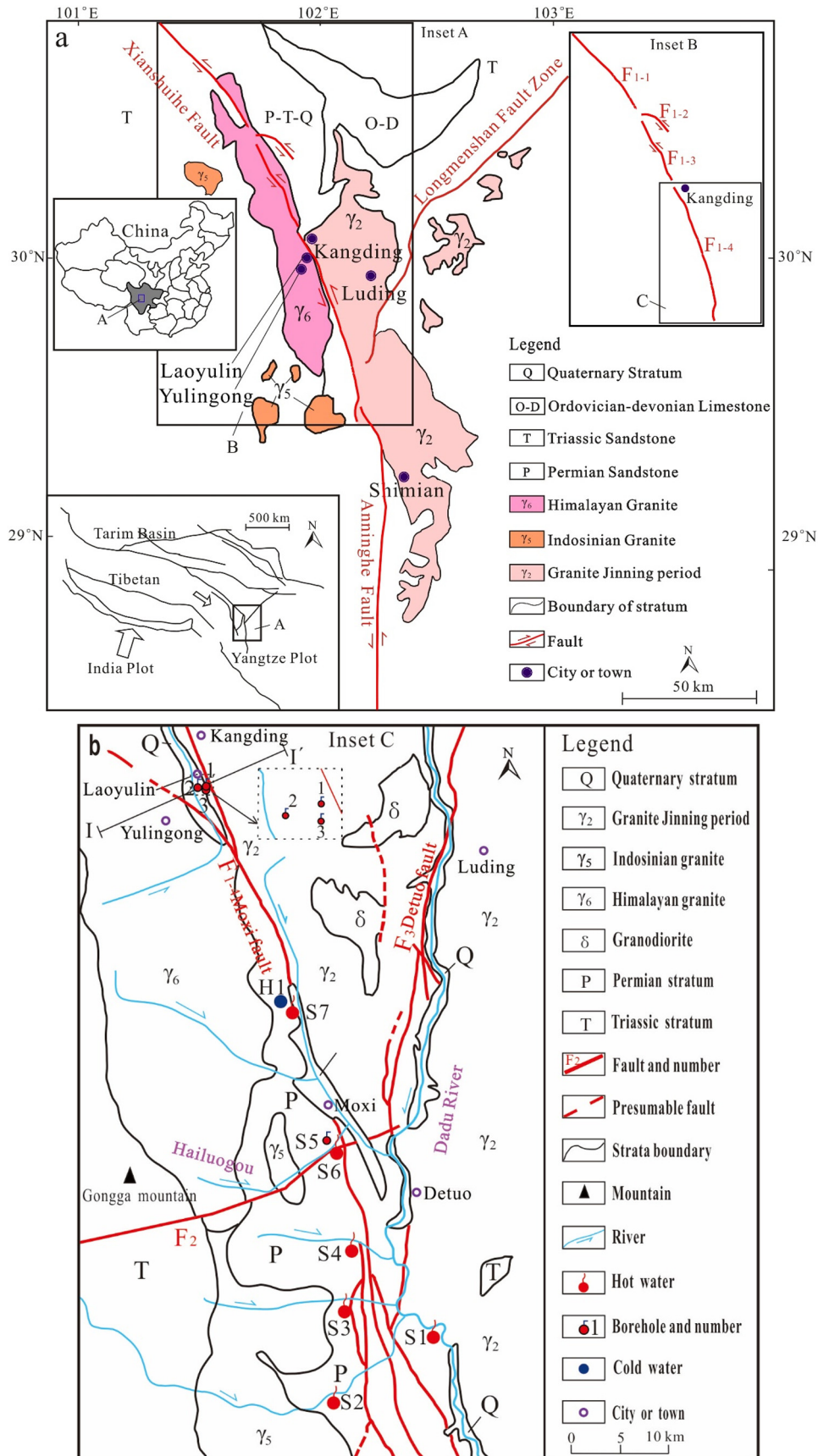
Fig. 1. Geological background map for the Moxi geothermal system in southern Sichuan Province. a. Simplified geological map of western Sichuan Province, China; the study area along the Moxi fault is located at the intersection area of the Xianshuihe Fault, the Longmengshan Fault and the Anninghe Fault (Tan et al., 2010). The Xianshuihe fault has four segments: F_{1-1} Qianning fault, F_{1-2} Yalahe fault, F_{1-3} Selaha fault and F_{1-4} Moxi fault. b. Regional geological map from Laoyulin located to the south of Kangding to Simian; F_1 is the Moxi fault, F_2 is the Hailuogou fault and F_3 is the Detuo fault; the cross section I-I′ is shown in Fig. 2.

occurs exactly at the junction of the Devonian and the Permian metamorphic, while Shenyuehe and Caoke springs, with lower temperatures and higher flow rates emerge from the Permian metamorphic rock and the crystalline lime stone, respectively.

Unlike the other springs, Wajiao Spring is exposed in Proterozoic magmatic rock with water at 35.2 °C high, and is located on the left bank of the Dadu River flowing through the eastern part of the intersection of the Moxi and Deto faults, approximately 5 km away from the main Moxi fault zone.

2.3. Conceptual model

The flow system is controlled by the Moxi fault, which cuts deep into the crust, and reaches the asthenosphere. The fracture zone, tens to hundreds wide in this area, is considered to contain fast paths for water and heat flows; thus, the flow system can be conceptualized as well connected to the deep heat source through the deep fault. It is expected that the Curie surface is about 17–25 km deep in this area because faults move frequently (Gao et al., 2015). Because the Curie temperature is 585 °C (Wu, 2013; Zhang et al., 2000), it follows that geothermal water is gradually elevated in temperature as it goes deeper and can reach a supercritical condition with temperatures of 374 °C or higher at a certain depth. Water descending along the fault and fractures can have high temperatures, high pressures and lower densities, so that the warmer water is driven up by its buoyancy (Fig. 2).

In the study area, many secondary faults extending east-west intersect the Moxi fault and provide advantageous zones for the rising hot water. Meanwhile, the cool waters near the ground surface replenish all types of deep flows and lower the water temperatures. Noticeably, solid tides influence the flow by rock deformation, which is more intensive in the deeper crust.

3. Method

Field investigations were performed on May 21, and Nov 10–20, 2015. Water samples were measured for physical parameters such as pH, oxidation-reduction Potential (ORP), dissolved oxygen (DO), and electrical conductivity (EC) using a WTW multi 3400i pH/EC/DO/ORP portable field meter in situ. The probes had been properly maintained, and the pH probe was calibrated before field measurements. HCO_3^- was determined by Gran titration with 0.025 N HCl.

Water samples were collected and preserved in550-ml polyethylene bottles. Before sampling, these bottles were washed and rinsed at least three times. Cation samples were acidified to less than 1 pH with concentrated reagent HCl acid. All experiments were performed within 21 days in the State Key Laboratory of Geohazard Prevention and Geo-environment Protection, Chengdu University of Technology. Cations were analyzed by ICP-OES (ICAP6300) with a precision of better than 10e-9 and anions by DIONEX (ICS-1100) with a precision of better than 10e-9.

For sulfite content, a 5-liter polyethylene container was used to collect thermal water, and reagent zinc acetate powder was added to the container. NaOH powder was added to the sample to bring the pH > 12 to facilitate precipitation of ZnS. After 24 h, the ZnS had accumulated at the bottom of the container and could be collected through filters.

4. Daily variations of geothermal flow

Two geothermal springs were chosen to be monitored for daily variations in temperature, flow rate, and physicochemical parameters such as pH, conductivity, DO, and ORP. One monitored spring, labeled S5, is located on the left bank of the Hailuogou, and the other is labeled S3 emerges on the left bank of the Shiyuehe river,
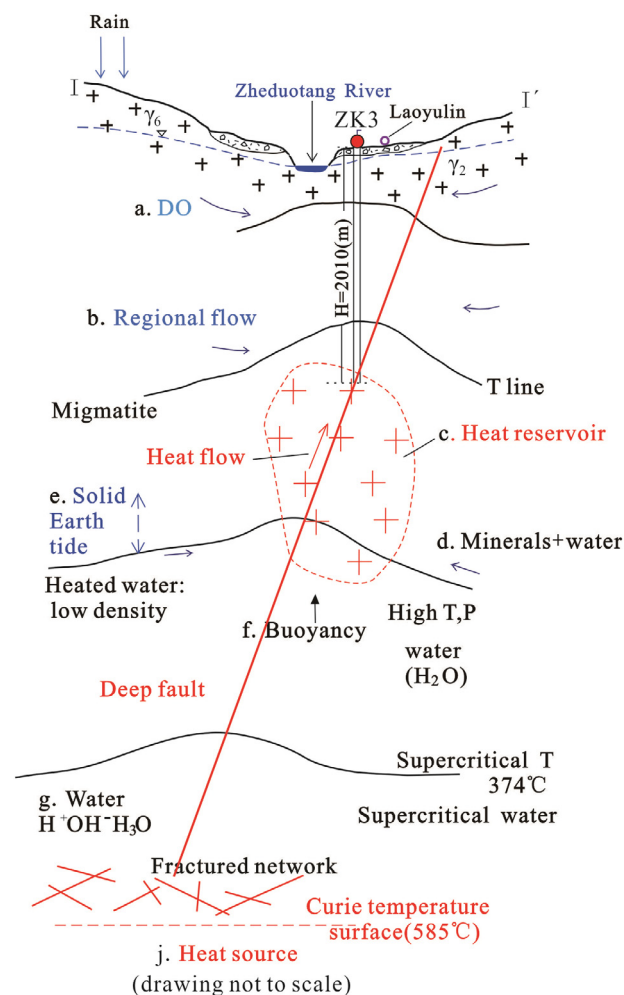

Fig. 2. Conceptual model of geothermal flow along the Moxi fault. The section shown in this figure is conceptualized as the Moxi fault plane, and the faults shown in this figure are the sub-faults such as the Hailuogou fault, which provide advantageous zones for hot water to discharge. a. DO is supplied in the shallow earth; b Regional flow can go deeply along the fault zone; c:The heat reservoir is migmatite, where groundwater can be heated; d: Migmatite can yield special minerals to groundwater by rock-water reactions; e: In deep ground, the solid earth tides can make the flows vary clearly; f: Heated flows with low density can be driven up by buoyancy; g: When the water is heated to 374 °C, it becomes supercritical water.

with the two providing different geothermal activity along faults extending southward (Fig. 1b). For comparison purposes, daily monitoring was carried out in May as the drought period and in December as the normal period.

A two-peak pattern in the 24-h cycle was shown in both periods at S5 (Fig. 3a and b), but the peak times are different. In May, it has one peak at approximately 8 pm at night and another at 9 am on the next day. In December, there is one at 5 pm and another at 5 am the next morning. It is interesting that the time gaps between the two peaks both are both approximately 12 h. It is well known that the air and ground temperatures are highest in the afternoon, and lowest in the morning before the sun rises, which may influence the temperature monitoring. However, it was found that the peak time did not remain consistent with this finding; the first one has a peak at 8 at night when the air is cooler in the afternoon, and the second one has a peak at 5 in the morning when the air may be the coolest of the entire day. Thus, we conclude that the air and ground temperature variations are not the main influence on the temperature variations of geothermal water. Similarly, the flow rate variations in the two periods also have a two-peak pattern.
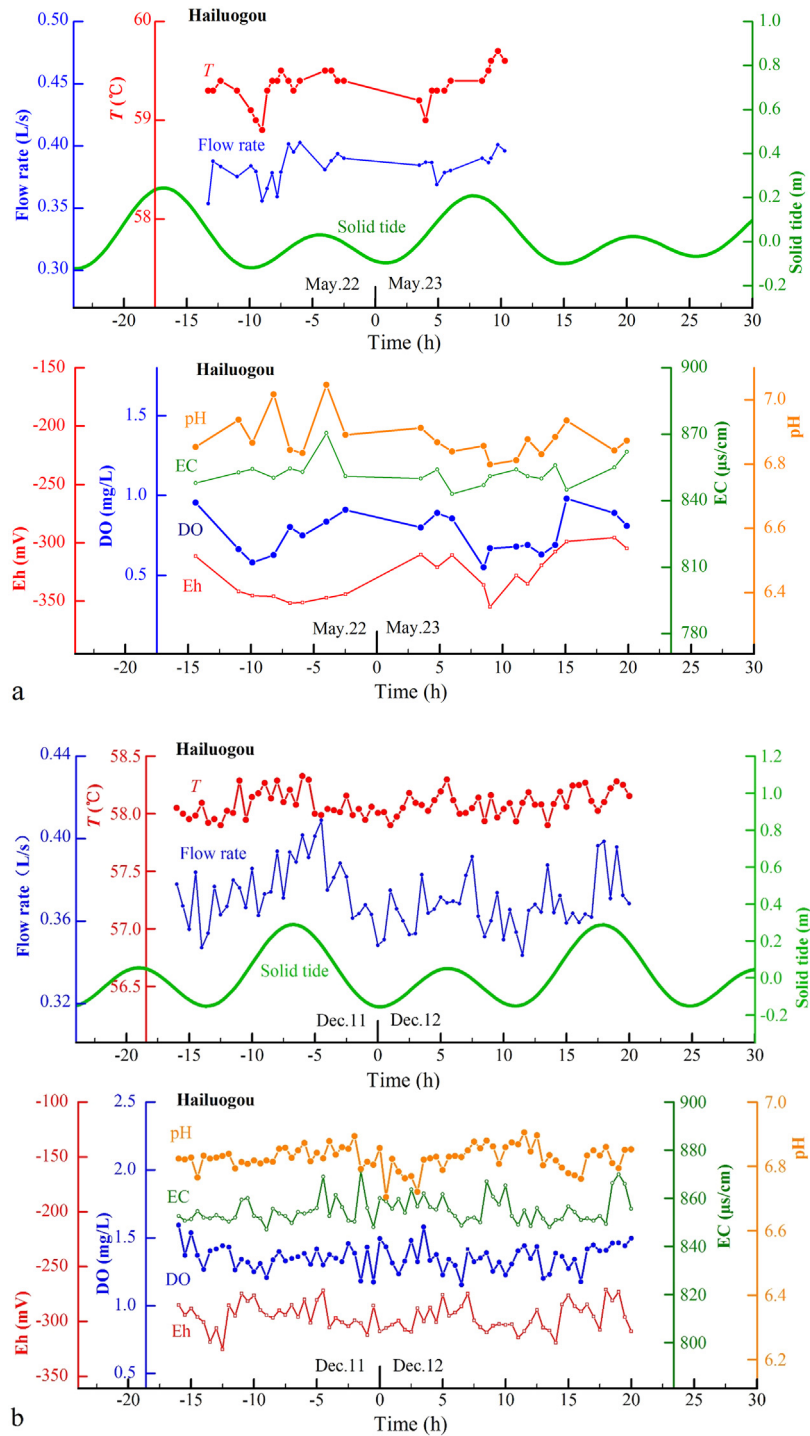
Fig. 3. Daily variations of temperature, flow rate, and physicochemical parameters for S5 located in Hailuogou (Fig. 1b). a. Variations in from May 22 to 23 in the drought season. The monitoring period for flow rate and temperature is shorter than that for physicochemical parameters, only 24 h long; b. Variations from December 11 to 12 in the normal season, the period of flow rate and temperature is similar to that for physicochemical parameters. The solid tide is calculated from a program from the International Earth Rotational and Reference Systems Series (IERS).

It is noted that the temperature changes during these two periods are different; the first one with approximately 1.0 °C is larger than the second one with 0.42 °C. Changes can also seen in the flow rate variations; the change in May of approximately 16.0% is larger than that in December at approximately 12.2%. Similar variations show that the flow rate is related to the geothermal temperature, which probably indicates that outflow volume is influenced by temperature (Lu and Liu, 2015).

In the same time period in December, the temperature and flow rate of S3 both show a two-peak pattern, and the peaks appear simultaneously with those of S5. However, the temperature change is only 0.25 °C, and the flow rate change is approximately 9.0%, which are lower values than those of S5 (Fig. 4).

These daily variations are further examined by comparison against the local solid tides, with some correlation appearing between them. The larger variations occur almost simultaneously
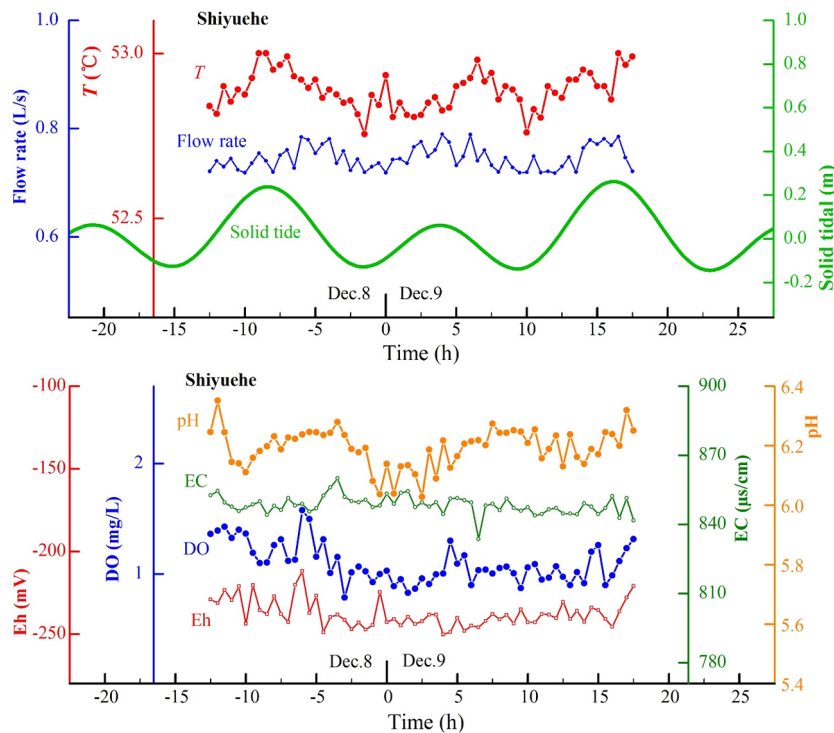
Fig. 4. Daily variations of temperature, flow rates, and physiochemical parameters for S3 located on the left bank of Shiyuehe (Fig. 1b) from December 8 to 9 in the normal season. The period for flow rate and temperature is similar to that for physicochemical parameters. The solid tide is calculated from a program from the International Earth Rotational and Reference Systems Series (IERS).

with the times when the solid tide becomes stronger; it can explain why the change in May is relatively higher than in December. For both the S5 and the S3 springs, the response is delayed, which can be utilized to trace the circulation of hot springs.

5. Aqueous chemistry

5.1. Aqueous chemistry

Six thermal springs and four boreholes were sampled and analyzed (Table 1), while surface water was sampled from a small river for comparison. Thermal springs showed weak alkalinity and acidity, as pH varied from 6.47 to 8.00, except in S1 which was 9.0, while the borehole waters in Laoyulin had a the higher pH range from 7.59 to 8.0.

The discharge temperatures of geothermal springs varied from 47 to 62 °C except in S1, which was only 35.2 °C far below the others, showing a downward trend to the south. Meanwhile, the temperature of the mixture of steam and water in boreholes reached 218 °C.

The ORP of geothermal waters varied from -35 to -392 mV, showing a negative oxidation-reduction potential. Similarly, the DO levels in the outflows were much lower than that of surface water and were lower than 1.0 mg/L for northern springs. It shows geothermal water originates under from very negative conditions and is influenced weakly by the cold waters.

The main anion of all geothermal water samples is HCO_3^- (Fig. 5), associated with discharges of CO_2 from the degassing effect (Wernera et al., 2008). When CO_2 increases, more dissolves in the reservoir, which can make the pH range from 6.0 to 6.5,and pH can rise to approximately 8.00 when temperature and pressure decrease on the way to the ground surface.

For the borehole waters, Cl^- is also prominent, and the SO_4^{2-} content rises for some springs located in the southern zone. For

Table 1
Physicochemical properties of water samples from the Moxi fault.

Water styles	No	Locations of springs	T (°C)	pH	Flow (L/s)	TS[b] (g/L)	ORP (mV)	DO (mg/L)	EC (μS/cm)	Hydro-chemical types
Thermal spring	S1	Wajiao	35.2	9.00	0.20	0.39	−35	2.20	188	Na-Ca-HCO₃
	S2	Caoke	47.0	7.10	1.50	0.73	−91	2.22	715	Ca-Na-HCO₃-SO₄
	S3	Shiyuehe	52.3	6.90	2.00	0.68	−228	1.46	1577	Ca-Na-HCO₃-SO₄
	S4	Wandong	59.9	7.56	0.66	0.82	−189	3.99	2140	Na-HCO₃
	S6	Hailuogou	62.0	6.47	2.50	–	−345	0.89	870	Na-HCO₃
	S7	Jianjian Mount	47.0	7.13	1.46	0.96	−276	0.87	1463	Na-HCO₃
Borehole[a]	S5	Hailuogou	59.0	6.87	0.36	0.92	−297	0.58	874	Na-HCO₃
	ZK1	Laoyulin	209.0	7.59	41.71	–	−392	0.31	2706	Na-Cl-HCO₃
	ZK2		172.0	8.00	16.10	1.19	−363	0.22	2085	Na-Cl-HCO₃
	ZK3		218.0	7.90	61.97	–	−374	0.40	2410	Na-Cl-HCO₃
River	H1	Jianjian Mount	27.9	8.10	0.2	–	15	5.55	207	Ca-HCO₃

[a] Borehole temperatures for ZK1, ZK2 and ZK3 deep in Laoyulin come from mixture of steam and water from boreholes at 267.3, 109.2 and 2010.0 m respectively, and the pressures of the borehole orifices when the mixtures were released were 1.05, 0.14, and 0.85 MPa respectively; other physicochemical data come from the borehole condensate waters. (Sampling was performed from December 8 to 10, 2015, with locations in Fig. 1b; dashed line represents lack of data).

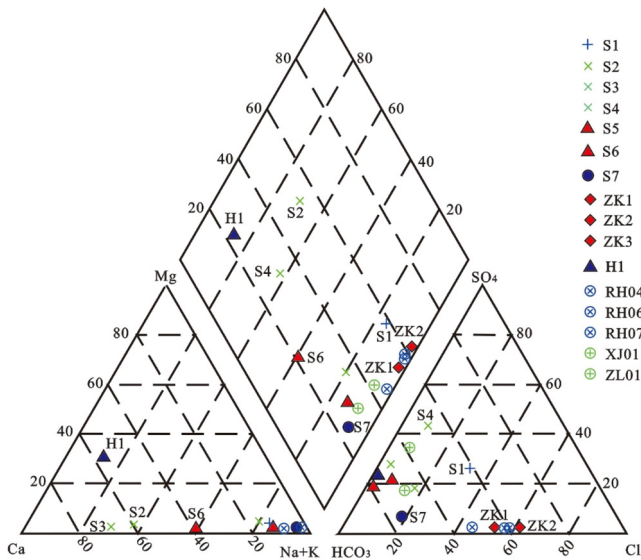[b] Sulfite concentrations (S^{2-}/HS^-) come from the ZnS deposition.

Fig. 5. Piper diagram for all water samples from the Moxi fault. Samples RH04 and Rh06 come from Rehai, Tengcong, Yunnan Province (Guo and Wang, 2012), and samples the XJ01 and ZL01 come from the Xijiang and Zenglong geothermal fields, respectively, in Guangdong Province (Lu and Liu, 2015).

the springs with higher SO_4^-, Ca^{2+} is the main cation, while for most springs, the main cation is Na^+.

It should be noted that F^- content is very high in most geothermal springs, which indicates that the water flows through igneous rock. Regarding the geothermal water of the southern zone, more water-rock reaction progress is expected as the deposits weather. B^- is the best element for tracing the influence of magma. Indeed, the B^- content is very high in several samples appearing in the northern zone, by which it can be inferred that the fault cuts deeply to the asthenosphere and that the geothermal water is heated by deep heat. Meanwhile, the B^- content decrease southward, indicating that the depth to which the geothermal water flows may be relatively shallower.
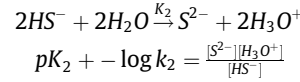
The hydrochemical types vary from Na-Cl-HCO_3 to Ca-Na-HCO_3-SO_4 (Table 1), as the central geothermal system near Laoyulin shows, and crystalline limestone maybe the sub-geothermal reservoir that causes the Ca^{2+} content to rise in southern springs.

5.2. S^{2-} content analysis

All geothermal waters have a strong sulfur odor, which may show that the springs are in a strong reducing environment. To quantify the sulfite concentration, we precipitated the sulfur from the samples by reagent zinc acetate power as soon as the geothermal water was taken, the procedure of ZnS precipitation noted above.

The sulfite content in the spring waters is shown in Table 1; it ranges from 0.68 to 1.19 g/L, and the highest content comes from the borehole water. High levels of sulfite content indicate a strong reducing environment in these springs, and the northern geothermal water at Laoyulin is stronger than those of the southern springs.

The HS^-/S^{2-} content of the geothermal water as gained from the ZnS deposition is shown in Table 1. The pH value at elevated temperatures calculated from the measured pH is lower in cold samples (Lu and Liu, 2015), such as 5 to 6, but the first and secondary ionization constants of H_2S are 1.16×10^{-7} and 9.5×10^{-14} respectively, at reservoir temperatures as high as 220 °C. Using the ionization constants and pH, the concentrations of HS^-/S^{2-} can be calculated according to the ionization Eq. (1).

$$H_2S + H_2O \xrightarrow{K_1} HS^- + H_3O^+$$
$$pK_1 + - \log k_1 = \frac{[HS^-][H_3O^+]}{[H_2S]}$$
$$2HS^- + 2H_2O \xrightarrow{K_2} S^{2-} + 2H_3O^+ \tag{1}$$
$$pK_2 + - \log k_2 = \frac{[S^{2-}][H_3O^+]}{[HS^-]}$$

The concentration of HS^- is approximately a few tens of milligrams per liter, and S^{2-} is approximately 10^{-8} ^{mg} per liter (Li and Zeng, 1983; Ling, 1985). Most of the hydrogen sulfide dissolves in water in the free molecular state but not as S^{2-}/HS^- in the natural environment. Because the ZnS precipitation occurred in samples with pH > 12, which is different from that of the natural environment, the HS^-/S^{2-} content cannot be shown in Table 2.

The equilibrium constant of the HS^- oxidation reaction in Eq. (2) is 4.1×10^{-121} in 25 °C (Li and Zeng, 1983; Ling, 1985), and it would decrease with rising temperature because the reaction releases much heat.

$$HS^- + 2O_2 + H_2O \xrightarrow{K_3} SO_4^{2-} + H_3^+O$$
$$pK_3 = - \log K_3 = \frac{[SO_4^{2-}][H^+]}{[HS^-][O_2]^2} \tag{2}$$
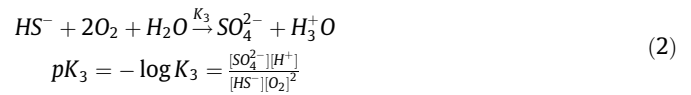
Most of the SO_4^{2-} in southern samples cannot come from HS^- oxidation, but perhaps comes from the mixing of cool water, which weakly influences the geothermal water from the borehole.

6. Deep temperature at groundwater circulation

6.1. Geothermal temperature

The reservoir temperature can be calculated by various geothermometers based on chemical composition such as the silica and alkali thermometry equations derived from the equilibrium constants of specific minerals and solutions, which have their applicable conditions. Silica dissolution is influenced weakly by pressure and salinity, and different silica thermometers can be used to calculate the reservoir temperatures of different cooling environments such as conductive cooling and steam loss (Arnórsson et al., 1983; Fournier, 1976). Meanwhile Na-K geothermometer is more suitable for estimating reservoir temperatures above 150 °C (Arnórsson et al., 1983).

All calculated temperatures (Table 3) are higher than discharge temperatures except for three borehole waters that were separated from the mixture of water and steam under a pressurized head. Thermal spring samples S2, S3 and S4 plot in the immature water zone of the triangular diagram for Na-K-$Mg^{1/2}$ (Fig. 6) and their K/Mg temperatures are much lower than their Na/K temperatures. This finding can be explained by geothermal water passing through sedimentary or crystalline limestone rock rich in Ca^{2+} and Mg^{2+} on the way to the ground surface, which causes the Mg^{2+} concentration to rise. Thus, the silica temperatures are considered more reliable than cation temperatures for the southern springs.

For S5 and S6, the calculated temperatures are similar, and plot in the zone of partially equilibrated or mixed zone waters. A similar result occurs with S7, but its temperature is higher and plots near the full equilibrium line in the triangular diagram.

The temperature of borehole ZK3, 2010 m deep, was measured when it was developed. Even at the depth of 1300 m, the gradient is nearly zero, and the temperature is constant to the bottom. It is not valid to use the average thermal gradient to evaluate the reservoir depth for a fault system with fast flow paths, heat convection and steam loss. Some researchers have conceived theoretical models to study the convection of a geothermal system in a faulted system. Rybach proposed a tube model to evaluate the geothermal reservoir depth of a convective type (Rybach, 1987). This model by Eq. (3), where T_s, T_r and T_0 represent the temperatures of

Table 2
Concentrations of major chemical components of geothermal spring water.

No.	Na	K	Mg	Ca	Cl⁻	SO_4^{2-}	HCO_3^-
S1	39.73	3.54	0.98	4.86	25.91	27.17	55.85
S2	47.78	2.85	2.30	95.99	30.58	182.71	249.32
S3	160.14	10.31	8.07	229.23	29.94	263.90	820.78
S4	315.86	11.16	9.95	53.61	100.22	142.53	650.14
S5	240.27	8.57	0.72	30.64	40.84	150.66	620.26
S6	150.51	4.56	0.53	86.43	12.18	111.12	580.03
S7	405.73	25.34	0.94	28.28	124.36	56.62	856.68
ZK1	954.04	96.52	1.86	3.51	875.13	22.18	895.41
ZK2	1023.45	100.12	0.61	0.23	895.68	24.39	909.22
ZK3	840.14	86.52	1.87	0.12	705.72	39.91	1006.90
H1	3.68	3.54	6.56	20.71	0.64	15.93	66.54

No.	Si	B	Li	Sr	Pb	F	Charge balance
S1	38.51	0.14	0.03	0.06	0.01	9.92	1.61%
S2	44.13	0.21	0.04	0.31	0.07	1.13	0.34%
S3	57.26	1.65	0.37	0.25	/	3.07	4.41%
S4	51.06	3.63	1.06	0.32	0.01	3.28	5.30%
S5	53.07	4.41	0.15	0.05	0.01	2.31	3.16%
S6	53.63	3.78	0.16	0.08	0.01	2.35	0.36%
S7	72.15	7.51	1.05	0.06	/	3.35	3.25%
ZK1	79.80	5.85	9.59	0.17	/	9.76	4.06%
ZK2	82.72	6.28	8.34	0.41	/	11.78	6.24%
ZK3	71.87	5.13	7.86	0.55	/	9.59	1.14%
H1	3.04	0.03	0.01	0.33	/	0.16	0.64%

Note: Charge balance (cations − anions)/(cations + anions); Samples from the Moxi fault; concentrations in mg/L with the exceptions of B, Li, and Pb in µg/L. Sample locations in Fig. 1b. The Pb concentrations of several samples are beyond detectable limits, shown by"/".

Table 3
Thermal reservoir temperatures estimated using Na/K, K/Mg and quartz geothermometers.

Sample No.	Temperature T (°C)[a]			
	Quartz[b]	Quartz[c]	Na-K	K-Mg
S1	82.5	88.3	198.1	68.6
S2	94.6	99.0	160.8	54.7
S3	122.76	123.5	166.0	54.7
S4	109.4	112.0	118.1	68.6
S5	113.7	115.2	118.2	94.4
S6	114.9	116.8	106.5	82.7
S7	121.6	122.6	163.4	121.8
ZK1	169.6	163.4	231.0	154.97
ZK2	171.2	164.7	227.2	177.6
ZK3	162.8	157.7	230.7	151.0

[a] Formulation based on Fournier (1976), Arnórsson et al. (1983) and Giggenbach (1988).
[b] Represents the temperature estimated by the quartz thermometer of silica-quartz conductive cooling (Fournier, 1976); t = 1390/(5.19 − log S) − 273.15, where S is the aqueous SiO_2 in mg/L.
[c] Represents the temperature estimated by the quartz thermometer after steam loss (Fournier, 1976; t = 1522/(5.75 − log S) − 273.15, where S is the aqueous SiO_2 in mg/L.

geothermal water, the reservoir temperature, and the cold water, respectively, v is the Darcy velocity, λ is the coefficient of heat conductivity of the rock, C is specific heat of water, and H is the geothermal reservoir depth.

$$\frac{(T_s - T_0)}{(T_r - T_0)} = \frac{2vC}{\pi\lambda H}\left[1 - \exp\left(\frac{-\pi\lambda H}{2v}\right)\right] \quad (3)$$

It is difficult to confirm these parameters, especially to the Darcy velocity, although some researchers proposed a method to evaluate it based on the temperature of the borehole (Bredehoeft and Papadulos, 1965) as showing in Eq. (4).

$$\frac{\partial^2 T}{\partial z^2} - \frac{\rho_f C}{\lambda} v \frac{\partial T}{\partial z} = 0 \quad (4)$$

Here, z is the depth in the borehole, and ρ is the density of geothermal water. Because the temperature gradient is varied, and nearly zero to below a 1300-m depth, the Darcy velocity varies exceedingly, and it cannot be estimated when the temperature is constant. Some researchers consider that deep geothermal flow is connected with supercritical flow (Xu et al., 2014; Lu et al.,

2016), and Eq. (3) is not valid in this environment. Lu simulates the temperature distribution of deep geothermal water flow at the Xinzhou thermal spring field (Lu et al., 2016). However, the temperature of the bottom boundary must be assumed, which means that the depth of the geothermal reservoir must be set in this type of model.

6.2. Strontium isotopes as hydrological tracer

After reacting with different types of rocks, the water has different $^{87}Sr/^{86}Sr$ ratios. The ratios for geothermal waters can be used to evaluate and trace where the water has flowed. The relationship between 1/Sr and $^{87}Sr/^{86}Sr$ is shown in Fig. 7. There are two main comparison point, igneous and carbonate which are located on the line composed by different rocks and surface waters (Fig. 7).

Borehole waters have values ranging from 0.7211 to 0.7235, close to the igneous ratio, indicating that the water flowed through a large volume of igneous rocks in this area and that the Moxi fault should cut into igneous rocks under lying the Permian rock at Mount Jianjian. However, the value for S6 is 0.7162, which is lower than that of S5 coming from the Hailuogou borehole.
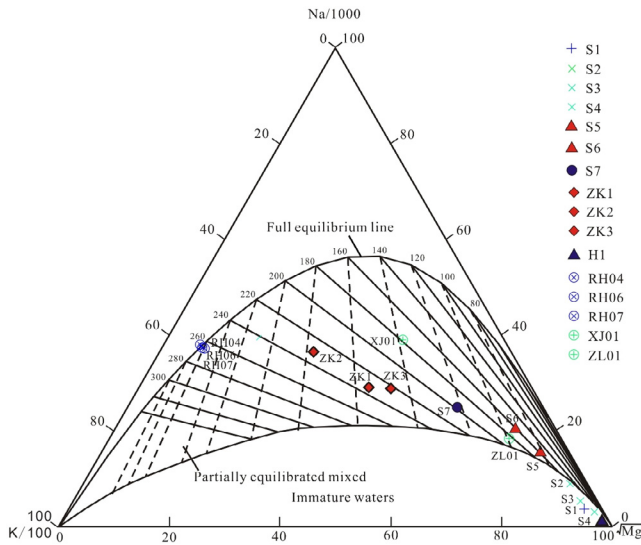
Fig. 6. Triangular diagram of Na-K-Mg$^{1/2}$ (from Giggenbach, 1988) for geothermal samples from the Moxi fault. Samples RH04, RH06 and RH07 come from the Rehai geothermal field, Yunnan Province (Guo and Wang, 2012); XJ01 comes from Xinyi's Xijiang geothermal field and ZL01 from the Zenglong geothermal field, Guangdong Province (Lu and Liu, 2015).
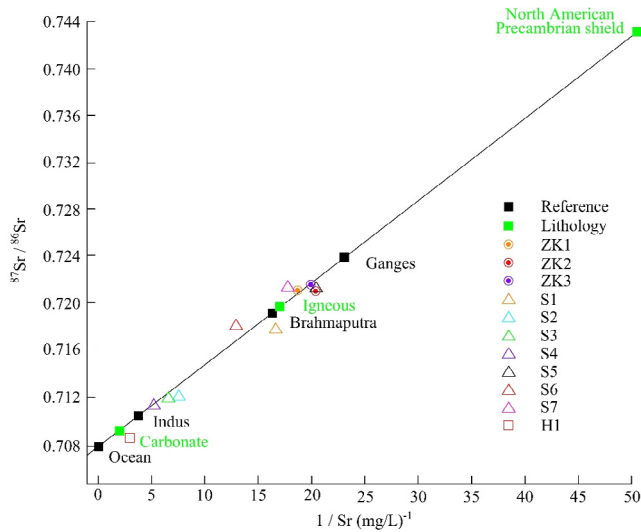

Fig. 7. Strontium isotopic tracers for hot spring waters from the Moxi fault in December 2015. Reference data from Fisher and Stueber (1976); Canadian Shield data from Millot et al. (2002) and Veizer (1989).

The ratio point is located between igneous and carbonate sedimentary rocks, signifying that water passed through both igneous rocks and sedimentary rocks. The other springs have $^{87}Sr/^{86}Sr$ values much lower than that of the Laoyulin's borehole water; they range from 0.7103 to 0.7121, near the carbonate value, probably indicating the reaction with crystalline limestone and Permian rock.

The low values of the river samples taken in the northern area indicate that the river flows mainly through Quaternary sedimentary rocks, which is consistent with the regional conditions. S1 occurs at the southern boundary of the study area, and it is a special one that has a 0.7182, which indicates that thermal water passed through igneous rocks as the Laoyuling borehole waters did. In fact, it appears in older, Indosinian magmatic rock. The variation of $^{87}Sr/^{86}Sr$ shows that, extending toward the south, the

water-rock reaction with igneous rocks becomes weaker, while reaction with sedimentary rocks becomes more stronger. Meanwhile S1 does not belong to the same geothermal system as the other springs.

7. Discussion

7.1. Geothermal water formation

Geothermal waters are distributed along the Moxi fault, which clearly cuts as deep as the asthenosphere (Fig. 1b). The temperature of outflows from the Laoyulin boreholes at approximately 2010 m deep can reach approximately 218 °C at 21.5 MPa (Table 1), but the natural spring nearby is approximately 81 °C at 0.1 MPa. It is implied that the temperature and pressure of geothermal waters decrease down quickly while they rise up to shallow ground. It takes only several weeks to rise this distance, and during this period, a new equilibrium cannot be achieved. Thus, the Na-K-Mg$^{1/2}$ triangular relationship (Fig. 6) shows partial equilibrium for the Laoyulin borehole water, S5, S6 and S7, which are distributed in the northern area. Theoretically, the more dissolved CO_2 arrives, the more Ca^{2+} and Mg^{2+} can enter the water at a lower temperature when it passes through the limestone exposed there (Eq. (5)). Meanwhile, it is more difficult for Na^+ and K^+ to achieve the equilibrium conditions because they require reaction times at a lower temperature. It probably indicates that the other springs are immature, exposed in Permian and Devonian crystalline limestones.

$$MCO_3 + CO_2 + H_2O \leftrightarrow M^{2+} + 2HCO_3 \qquad (5)$$

Moreover, B$^-$ has a lower value, implying that the t influence of deep heat becomes weaker in the southern geothermal system (Table 2). However, similar F$^-$ values for all springs show that granite is the main reservoir formation, in accordance with the geological background (Fig. 1).

The geothermal water can be viewed as heated by a deep source because it can release much CO_2 (Yang et al., 1999) and has a high B$^-$ content. The fracture zone makes it possible for internal crustal heat to transfer upward quickly to heat ground water. The water temperature is high with the lower geothermal gradient in the deeper part, and when the water goes up, the heat lost through advection by shallow groundwater causes the temperature to decrease rapidly.

7.2. Geothermal reservoir

The geothermal system is controlled by the Moxi fault, which is the boundary between Permian strata and Proterozoic granite. In fact, the younger granite of the Himalayan period is overlain by the Permian strata with lower permeability. The younger granite in the deep crust is speculated as the heat reservoir, which appears to be cooling and is cut into by the Moxi fault. Thus, the Permian strata become the cap rock of the reservoir.

The Moxi fault has a fracture zone 150–200 m wide and approximately 50 km long; meteoric water descends along the fracture zone from higher land driven by gravity (Fig. 2). It is the main geothermal reservoir, while the crystalline limestone may be minor in the southern system. The central of the geothermal area is near Laoyulin, and deep heat rises along the fractured fault zone. The farther away from the central zone, the weaker the thermal activities, as indicated by the thermometer according to the Na-K-Mg$^{1/2}$ relationship. Meanwhile, the reservoir temperature decreases toward the south. Although the reservoir depth cannot be calculated exactly, it still can be concluded that the depth becomes shallower with lower temperature lower. Further, the

reservoir unit is as the Himalayan granite exposed at the surface at Laoyulin.

7.3. Daily variations

Two sampling sites, S5 and S3, are chosen for variation monitoring because their volumes are relatively smaller, making it easier to use the volumetric method to monitor the flow rate for a short period at any time and obtain relatively accurate results. Moreover, their locations are widely separated to compare the northern and southern geothermal waters. The monitoring period is chosen as the 1st and 15th days in the lunar calendar because variation may become stronger, similar to the sea tidal cycle.

For these two springs, the variations of flow parameters have shown similar types of thermal water regimes. S5 might represent the dynamics of geothermal water that flows deeply, and is near to the central area of the Moxi deep fault thermal fields. The strong geothermal characteristics make the variation more prominent because it can reflect information from the deep earth.

The variation is comparatively weaker at S3 because it is near the boundary of the Moxi fault, where the fault might cut relatively lower, and the deep characteristics of the geothermal waters are possibly weaker possibly. The peak appearance is not associated with air and ground temperature peaks in the afternoon, showing that the variation is influenced weakly by the surroundings.

For both the S5 and S3 springs, the variation cycle between two peaks is approximately 12 h and is slightly delayed relative to the solid tides. It can be inferred that the fracture zone is a fast path for flow and heat. In times of high solid earth, the flow system becomes somewhat "open". The solid tide force works throughout the depth of the flow system. If the path reaches deeper, then the deformation is stronger, and the outflow variation is larger.

Certainly, the open path also makes heat transfer easier, resulting in a series of changes in chemical and physical parameters such as temperature and density. Theoretically, static conditions at 2.296 km deep could reach the critical pressure 22.5 MPa with gravity at 9.8 kg m/s^2 (Lu and Liu, 2015). The depth of borehole ZK3 nearly reaches the theoretical depth, and it is clear that the depth of the geothermal reservoir is greater than the depth of the borehole because the borehole temperature does not go down as far as the bottom. In addition, the depth of the heat reservoir of the Moxi fualt geothermal system should exceeds the theoretical depth.

Assuming a linear rise of geothermal temperature along depth along the local average geothermal gradient of 3.02 °C/100 m (Tan et al., 2010), the supercritical temperature would be reached at a depth of approximately 9.9 km, and the geothermal water temperature is approximately 218 °C at a 6 km depth. However, at the 1300-m depth of borehole ZK3, the temperature has almost risen up to 218 °C. Thus it can be inferred that the geothermal water, with very low negative ORP potential and low DO is related to deep-level supercritical hot water with strong reducing characteristics.

Although the geothermal water has been mixed with circulating groundwater, the variations of flow still contain information about the deep crust. Therefore, variations of flow have implications for earth quake monitoring, especially with respect to faults such as the Moxi fault that are strongly active at present..

8. Conclusions

This article discusses daily variations and aqueous chemistry of geothermal water flows occurring along the deep Moxi fault at the eastern edge of the Qinghai-Tibet plateau in western Sichuan Province, China. The report attempts to describe the geothermal for-

mation and groundwater circulation and to characterize the geothermal reservoirs.

It can be expected that the Moxi fault cuts deeply into the crust and the geothermal water is heated by deep heat sources. Based on the conceptual model, taking Curie temperature depths as 18–21 km (Gao et al., 2015) at 578 °C, we can estimate the average geothermal gradient as 3.4 °C /100 m, which is similar to the value used to calculate the depth of supercritical conditions. The high B$^-$ and F$^-$ contents in the thermal waters also show the deep circulation of the geothermal waters and could be influenced by magma.

We use a multi-process coupling approach with thermal, hydrological and chemical aspects to characterize the geothermal waters. Controlled by the Moxi fault, geothermal springs reflect water-rock mineral reactions, while mixing with circulating groundwater also changes the equilibrium conditions. The $^{87}Sr/^{86}Sr$ data have distinguished different water-rock reactions, consistent with the regional geological data and ion concentration variations. The northern geothermal water reacts mainly with igneous rocks, and the southern water is also influenced by crystalline limestones. Both flow variation analysis and aqueous chemistry study show that geothermal water probably comes from the deep crust, heated by magmatic heat. The heat focus of this geothermal system is likely located in the northern part of the Moxi fault near Laoyulin, with the southern boundary in Shimian. Extending southward along this fault, the circulation depth decreases, and geothermal water has weaker responses to solid tides, as suggested by the fact that the variation of S5 is stronger than the variation of S3. It infers that the cutting depth of the Moxi fault decreases from north to south. Meanwhile, the geothermal temperatures are reduced toward the south. The calculated temperature of Laoyulin can reach approximately 230 °C; other springs located in the partial equilibrium zone of the triangular diagram for Na-K-Mg$^{1/2}$ range from 120 to 160 °C, and the temperatures of the immature springs are below 120 °C.

Near Simian, the geothermal activity terminates where S1is located. S1 has different aqueous characteristics from the other springs and is not consistent with the variation rule from north to south. Its F$^-$ concentration is high, but its B$^-$ concentration is close to that of surface water, which shows that its heat source does not come from the deep crust.

The unique study contribution of these springs includes using supercritical water to analyze the characteristics of the flow. The geothermal water can become supercritical water because the fault cuts deeply and causes the geothermal temperature to exceed the supercritical temperature, and the buoyancy of this type of lower-density water pushes it to rise quickly along the fault.

Based on the researches noted above, the variation monitorings might hold the key to further understanding of the conditions and processes in the deep ground, and aqueous geochemistry provides encouraging prospects for expanding geothermal research to the region south of Kangding where earthquake activity is frequent and has received little attention.

The variations of geothermal flow delay the effects of the solid tide, but the interpretation for the delay is complex, and the lack of a quantified method makes earthquake forecasting difficult. More monitoring work for long periods and at more thermal springs could lead to a better understanding of the deep geothermal system along the Moxi fault.

for Kangding's Kangren geothermal company and two reviewer's comments' for improvements of the paper.

References

An, Y., 2010. Boundary features of the seismic rupture segments along the Xianshuihe Fault zone. Geological Institute of China. Doctor's degree (in Chinese with English abstract).

Arancibia, G., Fujita, K., Hoshino, K., Mitchell, T.M., Cembrano, J., Gomila, R., Morata, D., Faulkner, D.R., Rempe, M., 2014. Hydrothermal alteration in an exhumed crustal fault zone: Testing geochemical mobility in the Caleta Coloso Fault, Atacama Fault System, Northern Chile. Tectonophysics 623, 147–168.

Arnórsson, S., Gunnlaugsson, E., Svavarsson, H., 1983. The chemistry of geothermal waters in Iceland. III. Chemical geothermometry in geothermal investigations. Geochim. Cosmochim. Acta 47, 567–577.

Bredehoeft, J.D., Papadulos, I.S., 1965. Rates of vertical groundwater movement estimated from the earth's thermal profile. Water Resour. Res. 1 (2), 325–328.

Cao, Y., Li, H., Liu, Z., Yuan, D., Shen, L., 2006. Comparison of geochemical features of warm springs between Chongqing and Kangding. Carsologica Sin. 25 (2), 112–120 (in Chinese with English abstract).

Capecchiacci, F., Tassi, F., Vaselli, O., Bicocchi, G., Cabassi, J., Giannini, L., Nisi, B., Chicciora, G., 2015. A combined geochemical and isotopic study of the fluids discharged from the Montecatini thermal system (NW Tuscany, Italy). Appl. Geochem. 59, 33–46.

Fisher, R.S., Stueber, A.M., 1976. Strontium isotopes in selected streams within the susquehanna river basin. Water Resour. Res. 12, 1061–1068.

Fournier, R.O., 1976. Estimates of temperatures and salinities of aquifers in geothermal system at Cerro-Prieto, Mexico from Hot–spring Date. Geol. Soc. Am. 8, 873–874.

Gao, L., Zhang, J., Dong, M., 2015. The study of gravity–magnetic anomaly and tectonic background in Sichuan west region. Chin. J. Geophys. 58 (8), 2996–3007 (in Chinese with English abstract).

Giggenbach, W.F., 1988. Geothermal solute equilibria. Derivation of Na–K–Mg–Ca geoindicator. Geochem. Casmochem. Acta 52 (2), 2749–2765.

Guo, Q., 2012. Hydrogeochemistry of high-temperature geothermal systems in China: a review. Appl. Geochem. 27 (10), 1887–1898.

Guo, Q., Wang, Y., 2012. Geochemistry of hot springs in the Tengchong hydrothermal areas, Southwestern China. J. Volcanol. Geotherm. Res. 215–216, 61–73.

Humphris, S.E., Tivey, M.K., Tivey, M.A., 2015. The Trans-Atlantic Geotraverse hydrothermal field: a hydrothermal system on an active detachment fault. Deep Sea Res. II 121, 8–16.

Kaasalainen, H., Stefánsson, A., Giroud, N., Arnórsson, S., 2015. The geochemistry of trace elements in geothermal fluids, Iceland. Appl. Geochem. 62, 207–223.

Kalacheva, E., Taran, Y., Kotenko, T., 2015. Geochemistry and solute fluxes of volcano–hydrothermal systems of Shiashkotan, Kuril Islands. J. Volcanol. Geotherm. Res. 296, 40–54.

Khaska, M., Le Gal La Salle, C., Videau, G., Flinois, J.S., Frape, S., Team, A., Verdoux, P., 2015. Deep water circulation at the northern Pyrenean thrust: Implication of high temperature water–rock interaction process on the mineralization of major spring water in an overthrust area. Chem. Geol. 419, 114–131.

Khutorskoi, M.D., Polyak, B.G., 2014. Geothermal models of various geodymanic settings. Geotectonics 48 (1), 68–85.

Lee, S.G., Kim, T.K., Lee, T.J., 2011. Strontium isotope geochemistry and its geochemical implication from hot spring waters in South Korea. J. Volcanol. Geotherm. Res. 208 (1–2), 12–22.

Li, X., Shibazaki, B., 2014. 3D modeling of earthquake cycles of the Xianshuihe fault, southwestern China. J. Asian Earth Sci. 96, 205–212.

Li, S., Zeng, Q., 1983. Physical Chemistry. Higher Education Press (in Chinese).

Ling, C., 1985. Handbook of Thermodynamic Data of Compounds (in Chinese).

Liao, Z., Zhao, P., 1999. Yunnan-Tibet Geothermal Belt-Geothermal Resources and Case Histories. Science Press (in Chinese).

Liu, C., Zhu, B., Yang, X., Shi, Y., 2016. Geodynamic background of the 2008 Wenchuan earthquake based on 3D visco-elastic numerical modelling. Phys. Earth Inter. 252, 23–36.

Lu, G., Wang, X., Xu, F., Li, F., Wang, Y., Qi, S., Yuen, D., 2016. Deep geothermal processes act through deep fault and solid tide in Xinzhou geothermal field in coastal Guangdong, China. Phys. Earth Planet. Inter. (this issue)

Lu, G., Liu, R., 2015. Aqueous Chemistry of typical geothermal springs with deep faults in Xinyi and Fengshun in Gunangdong Province, China. J. Earth Sci. 26 (1), 60–72.

Luo, G., Liu, M., 2010. Stress evolution and fault interactions before and after the 2008 Great Wenchuan earthquake. Tectonophysics 491 (1–4), 127–140.

Mao, X., Wang, Y., Yuan, J., 2013. The indication of geothermal events by helium and carbon isotopes of hydrothermal fluids in South China. Proc. Earth Planet. Sci. 7, 550–553.

Mao, X., Wang, Y., Zhan, H., Feng, L., 2015. Geochemical and isotopic characteristics of geothermal springs hosted by deep-seated faults in Dongguan Basin, Southern China. J. Geochem. Explor. 158, 112–121.

Millot, R., Gaillardet, J., Dupré, B., Allègre, C., 2002. The global control of silicate weathering rates and the coupling with physical erosion: new insights from rivers of Canadian shield. Earth Planet. Sci. Lett. 196, 83–98.

Mohammadi, Z., Bagheri, R., Jahanshahi, R., 2010. Hydrogeochemistry and geothermometry of Changal thermal springs, Zagros region, Iran. Geothermics 39 (3), 242–249.

Navarro-Ciurana, D., Corbella, M., Cardellach, E., Vindel, E., Gómez-Gras, D., Griera, A., 2016. Petrography and geochemistry of fault–controlled hydrothermal dolomites in the Riópar area (Prebetic Zone, SE Spain). Mar. Pet. Geol. 71, 310–328.

Pang, Z., Yuan, L., Huang, T., Kong, Y., Liu, J., Li, Y., 2013. Impacts of human activities on the occurrence of groundwater nitrate in an alluvial plain: a multiple isotopic tracers approach. J. Earth Sci. 24 (1), 111–124.

Phuong, N.K., Harijoko, A., Itoi, R., Unoki, Y., 2012. Water geochemistry and soil gas survey at Ungaran geothermal field, central Java, Indonesia. J. Volcanol. Geotherm. Res. 229–230, 23–33.

Reed, M.H., 1982. Calculation of multicomponent chemical equilibria and reaction processes in systems involving minerals, gases and an aqueous phase. Geochim. Cosmochim. Acta 46 (4), 513–528.

Rissmann, C., Nicol, A., Cole, J., Kennedy, B., Fairley, J., Christenson, B., Leybourne, M., Milicich, S., Ring, U., Gravley, D., 2011. Fluid flow associated with silicic lava domes and faults, Ohaaki hydrothermal field, New Zealand. J. Volcanol. Geotherm. Res. 204, 12–26.

Rybach, L., 1987. Geothermal sysem, conductive heat flow and geothermal anomalies. In: Rybach, Muffler (Eds.), Geothermal Systems, Principals and Case Histories. John Wiley & Sons Ltd..

Shakeri, A., Ghoreyshinia, S., Mehrabi, B., Delavari, M., 2015. Rare earth elements geochemistry in springs from Taftan geothermal area SE Iran. J. Volcanol. Geotherm. Res. 304, 49–61.

Shan, B., Xiong, X., Wang, R., Zheng, Y., Yang, S., 2013. Coulomb stress evolution along Xianshuihe-Xiaojiang Fault System since 1713 and its interaction with Wenchuan earthquake, May 12, 2008. Earth Planet. Sci. Lett. 377–378, 199–210.

Shao, Z., Xu, J., Ma, H., Zhang, L., 2016. Coulomb stress evolution over the past 200 years and seismic hazard along the Xianshuihe fault zone of Sichuan, China. Tectonophysics 670, 48–65.

Sheng, L., 2007. The study of deep sorce CO_2 degasification and carbon cycle in the southwest of China. Southwest Jiao Tong University. Doctor's degree (in Chinese with English abstract).

Shi, Z., Wang, G., 2013. Relationship between the Earth tidal factor and phase lag of groundwater levels in confined aquifers and the Wenchuan Ms8.0 earthquake of 2008. Sci. China Earth Sci. 43 (7), 1132–1140.

Tan, X., Xu, X., Lee, Y., Chen, G., Wan, J., 2010. Apatite fission track evidence for rapid uplift of the Gongga Mountain and discussion of its mechanism. Chin. J. Geophys. 53 (8), 1859–1867 (in Chinese with English abstract).

Tassi, F., Aguilera, F., Darrah, T., Vaselli, O., Capaccioni, B., Poreda, R.J., Huertas, A.D., 2010. Fluid geochemistry of hydrothermal systems in the Arica-Parinacota, Tarapacá and Antofagasta regions (northern Chile). J. Volcanol. Geotherm. Res. 192, 1–15.

Veizer, J., 1989. Strontium isotopes in Seawater through time. Annu. Rev. Earth Planet. Sci. 17, 141–167.

Wang, S., Pang, Z., Liu, J., Lin, P., Liu, S., Yin, M., 2013. Origin and evolution characteristics of geothermal water in the Niutuozhen geothermal field, North China Plain. J. Earth Sci. 24, 891–902.

Wei, M., Tian, T., Sun, Y., Li, X., 2012. A study of the scaling trend of thermal groundwater in Kangding county of Sichuan. Hydrogeol. Eng. Geol. 39 (5), 132–138 (in Chinese with English abstract).

Wernera, C., Hurwitzb, S., Evansb, W.C., Lowensternb, J.B., Bergfeldb, D., Heaslerc, H., Jaworowskic, C., Huntd, A., 2008. Volatile emissions and gas geochemistry of Hot Spring Basin, Yellowstone National Park, USA. J. Volcanol. Geotherm. Res. 178, 751–762.

Wu, Z., 2013. Application of comprehensive geophysical methods to prospecting of Yangjiang's Xinzhou geothermal field. In: International Workshop on Exploration & Development of Geothermal Resource in Guangdong. Guangdong Geological Bureau and China University of Geosciense (Wuhan), Guangzhou.

Xu, T., Feng, G., Shi, Y., 2014. On fluid-rock chemical interaciton in CO_2-based geothermal system. J. Geochem. Explor. 144, 179–193.

Yaguchi, M., Muramatsu, Y., Chiba, H., Okumura, F., Ohba, T., Yamamuro, M., 2014. Hydrochemistry and isotopic characteristics of non-volcanic hot springs around the Miocene Kofu granitic complex surrounding the Kofu Basin in the South Fossa Magna region, central Honshu, Japan. Geochem. J. 48, 345–356.

Yang, T., Fu, C., Walia, V., et al., 2006. Seismo-geochemical variations in SW Taiwan: multi-parameter automatic gas monitoring results. Pure Appl. Geophys. 163 (4), 693–709.

Yang, L., Wei, J., Sun, J., 1999. A study of the deep-source CO_2 release of hot springs system in Kangding. Acta Geol. Sin. 73 (3), 278–285 (in Chinese with English abstract).

Zhang, G., Hetland, E.A., Shan, X., Vallée, M., Liu, Y., Zhang, Y., Qu, C., 2016. Triggered slip on a back reverse fault in the Mw6.8 2013 Lushan, China earthquake revealed by joint inversion of local strong motion accelerograms and geodetic measurements. Tectonophysics 672–673, 24–33.

Zhang, W., 1978. The Developments of Fracture-systems in China. The International Exchange of Geological Research Papers. Geological Press (in Chinese).

Zhang, S., Liu, M., Hu, X., 2000. Re-study of currier temperature surface and seismic activity in Northern China region. Geophys. Geochem. Explor. 24, 81–86.

Zhao, Q., 1984. Water hydrology geochemistry characteristics of the water in the fracture zone of Xianshuihe fault. J. Chengdu Univ. Sci. Technol. 2, 77–88 (in Chinese with English abstract).

Zhou, X., 2011. Gas geochemistryin western Sichuan related to 12 May 2008 Wenchuan Ms8.0 earthquake. University of Science and Technology of China. Doctor's degree (in Chinese with English abstract).